



ORIGINAL PAPER

DELINEATING STRUCTURE ELEMENTS AND DEPTH OF SOURCES USING AN AEROMAGNETIC DATASET IN THE TARHONA REGION, NORTHWEST LIBYA**Fouzie TREPIL^{1,2)}, Nordiana Mohd MUZTAZA¹⁾, *, Ismail Ahmad ABIR¹⁾, Mohamed A. SALEEM³⁾, Siti ZULAIKAH⁴⁾ and Teoh Ying JIA¹⁾**¹⁾ School of Physics, Universiti Sains Malaysia 11800, Pulau Penang, Malaysia²⁾ Geophysics Dept., Faculty of Science, University of Tripoli, PO Box 13275, Tripoli, Libya³⁾ Petroleum Institute, Tripoli, 6431, Libya⁴⁾ Faculty of Mathematic and Natural Sciences, Universitas Negeri Malang, Indonesia*Corresponding author's e-mail: mmnordiana@usm.my**ARTICLE INFO****Article history:**

Received 4 May 2023

Accepted 11 July 2023

Available online 20 July 2023

Keywords:

Magnetic

Tarhona

Structure

Fault system

Libya

ABSTRACT

The Tarhona region, which is situated within the northwestern part of Libya, is a part of Jabal Nafusah (eastern Jabal) due to its geographic location and the character of the escarpment. It is restricted to the east by longitudes 13.00° to 14.00° east and to the north by latitudes 31.45° to 32.25° north. The analysis and interpretation of magnetic data can depict previously unknown regions and improve scientific knowledge of the study area. However, the geological ambiguity of the study area makes it challenging to figure out the geological interpretation within and around the area. Therefore, this study aims to delineate structural elements and depths of sources using an aeromagnetic dataset in the Tarhona region in northwest Libya. Magnetic dataset is reduced to the pole (RTP) within Oasis Montaj. Different filters were utilised to magnetic data, including Total horizontal gradient (THG), CET grid analysis, Power spectrum analysis (PS), Analytic signal (AS), 3D Euler deconvolution (ED), and Tilt derivative (TDR). The result shows various fault tendencies in the N-S, NNW-SSE, and NW-SE directions. The depth of faults was determined from 2000 to above 8000 m after applying 3D Euler deconvolution with the TDR derivative. In addition, a rose diagram was prepared for delineating the trend of the faults using edge detection techniques (THG, CET grid analysis, AS, Euler deconvolution, and TDR). The delineation of subsurface structures in the region is helpful for further hydrocarbon exploration.

1. INTRODUCTION

The ambiguity related to hydrocarbon identification can be significantly reduced through the combination of geological history with geophysical exploration techniques. Its combination can indeed increase the prospect of identifying elements of structure that control hydrocarbon accumulation in the region. In order to more effectively delineate geological elements, magnetic data is among the most valuable tools (Elkhateeb et al., 2018). The aeromagnetic approach (Vasanthi et al., 2006) is a faster, cheaper, and more versatile geophysical tool that has the potential to reveal regional-scale as well as smaller-scale features, including differences in magmatic intrusions, basement type, basement surface, volcanic rocks, and fault systems (Feumoe et al., 2012). According to Sharma (1997), magnetic data interpretation and improvement are used for distinguishing deep and shallow geological features (Eldosouky, 2019). Mapping structural features is essential to exploring hydrocarbon, geothermal, groundwater, and mineral resources (Masoud and Koike, 2011; Salehi et al., 2015). More so, understanding the rock units, faults, contacts, dykes, and lineaments is significant to the structural study

(Abdulkadir et al., 2022). Geophysical tools have numerous applications, including in archaeology, hydrogeology, engineering, ecology, tectonics, mineral deposits, hydrocarbon exploration, and other fields. Saadi et al. (2008) concluded that geophysical methods describe the physical properties of geological rocks beneath the surface. The Tarhona region (Fatmi et al., 1978), which is situated within the northwestern part of Libya, is a part of Jabal Nafusah (eastern Jabal) due to its geographic location and the character of the escarpment (Fig. 1). It is restricted to the east by longitudes 13.00° to 14.00° east and to the north by latitudes 31.45° to 32.25° north. Because the study area lies between two production basins, the Ghadames and Pelagian basins (Trepil et al., 2021), the Tarhona region is a promising area with the potential for hydrocarbon accumulation. In addition, the area is considered to be a structurally complex region of the fold belt of the Atlas due to various geological occurrences that exist within. The geological ambiguity of the study region makes it challenging to figure out the geological structures within and around the area. Unfortunately, understanding structural development is heretofore insufficient. Numerous geological and geophysical investigations have been

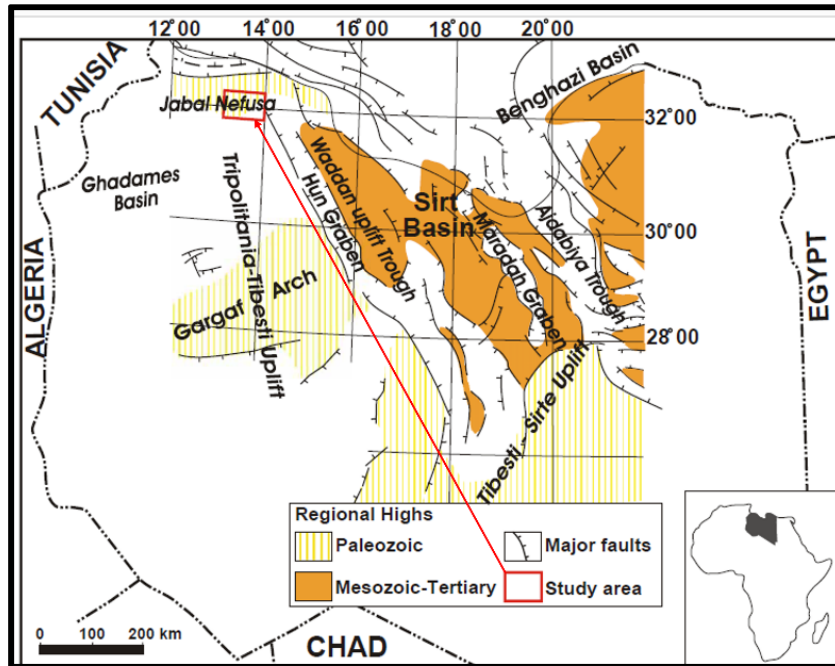


Fig. 1 The study area (red rectangular) superimposed on a tectonic map of Libya by Rusk (2001).

conducted in the Tarhona area and the adjacent area northwest of Libya, including gravity, and remote sensing data to understand the surface and subsurface structures (El Hinnawy and Cheshitev, 1975; Zivanovic, 1977; Saadi et al., 2008; Alfandi, 2012). Therefore, the investigation of geological structures provides significant insights into the history and development of the study region and the surrounding region, which are required for potential hydrocarbon exploration activities (Saadi et al., 2011). Within the Oasis Montaj programme, many filters are used to interpret the magnetic data, including reduction to the pole filter, Total horizontal gradient (THG), CET grid analysis, Power spectrum analysis (PS), Analytic signal (AS), 3D Euler deconvolution (ED), and Tilt derivative (TDR). Consequently, the aim of the study is to delineate the structural elements and source depths that exist in the Tarhona region of northwest Libya. Furthermore, the main results are useful for identifying new features that provide improved comprehension of the study area's structure.

GEOLOGICAL SETTING

The Tarhona area (Fatmi et al., 1978) is a part of Jabal Nafusah (eastern Jabal) due to its geographic location and the character of the escarpment. Furthermore, the Nafusah Uplift (also called the "Nafusah Arch"), shown in Figure 1 (Abohajar et al., 2009), is a major tectonic feature that extends from east to west and from northeast to southwest, which is the boundary between the Ghadames Basin in the north and the plain of Jifara (Trepil et al., 2021). According to Giraudi (2005), the Nafusah Arc is among the most distinctive morphological features in northwest Libya. Basins within northwest Africa

developed as the result of a Phanerozoic sequence of uplifts that intersected each other in diagonal directions, according to Klitzsch (1970) and Klitzsch and Gray (1971). Furthermore, he suggested that the Early Caledonian tectonic phase revitalised what was previously a weak suture zone with Pan-African origins. Accordingly, it appears that this is the origin of the common idea that uplifting is a part of the predominantly E-W trending "Nafusah arch". Farahat et al. (2006) concluded that large recent continental landmasses are frequently affected by neotectonic activity; this is typically related to mantle events during which uplift is created through rising plumes related to hot spots (Alfandi, 2012). The Garyan-Tarhona strip was uplifted in the upper Cretaceous or lower Tertiary, resulting in a NW-SE trending anticlinal swelling. Jabal Nafusah was considered to have been uplifted during the Hercynian orogenesis; this uplift was associated with northwest-southeast faulting. Further, joints within the Jabal Nafusah area have a broad NW trend that is contemporaneous with volcanism (Saadi et al., 2008). The strike of structure in the Hun Graben is NNW-related to the reactivation of Cretaceous features (Capitanio et al., 2011). Mann (1975) reported that the Jabal Nafusah's structural development ceased towards the upper Cretaceous. Northwest Libya as well as southern Tunisia are located close to the Saharan flexure or lineament, as described by Anketell (1996), who also located them on the eastern flank of the south Atlas fold belt (Alfandi, 2012). Generally, the majority of the Tarhona region is composed of broad plains formed by basalt sheets, which form flats, while the lower topography is mostly covered by fluvial-eolian deposits (Saadi et al., 2008). The

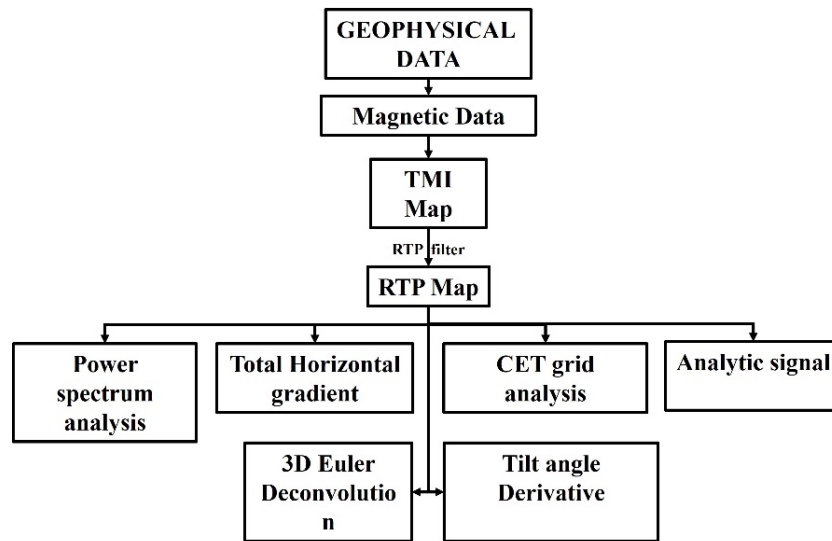


Fig. 2 The methodology flowchart.

Tarhona region consists of sedimentary rocks of clastic and carbonate composition (sandstone, limestone, clays, and marl) and their ages from the mid-to-upper Triassic to Quaternary. Volcanic activities in the late Cretaceous period generated Tertiary-Quaternary volcanic rocks that are present in the majority of the region (Hallett and Lowes, 2017). Basalt cones, basalt flows, trachyte, and phonolite intrusions are the three main forms of volcanic rocks in the region (Antonovic, 1977). Piccoli (1970) estimated that the basalt sheet formed between the early Eocene and the Pliocene. On the other hand, Christie (1966) thought the basalt within Wadi Ghan originated in the early Quaternary.

2. MATERIALS AND METHOD

2.1. MAGNETIC DATA

The magnetic approach (also referred to as the "geomagnetic method") is a geophysical technique that detects alterations in the Earth's magnetic field using variations in the rocks' magnetic susceptibility. It's a passive, non-destructive technique (Hinze et al., 2013). An aeromagnetic dataset is gathered from the AMMP (African Magnetic Mapping Project). The AMMP is a collaborative effort between P (Peterson), G (Grant), PGW (Watson Limited) in Canada, GETECH in the UK, the International Institute for Geo-Information Science, and ITC (Earth Observation) in the Netherlands. Both the flying lines as well as the dataset points along every line are spaced out by 1.0 kilometre. Approximately 8,798 magnetic datasets were collected, with 106 flight lines in the north-south direction and around 83 datasets collected along the entire flight line. Numerous scientists have applied aeromagnetic data, e.g., Feumoe et al. (2012) applied aeromagnetic data to delineate tectonic lineaments in the southeast Cameron area. Anudu et al. (2014) mapped intra-sedimentary volcanoes and delineated geologic

structures during the middle Cretaceous in the Benue Trough, Nigeria, utilising aeromagnetic data. Elkhateeb et al. (2018) delineated porphyry intrusions and structural complexity areas, and Eldosouky (2019) identified edge detection of geological contacts in the Samr El-Qaa region, NE Desert, Egypt, using an aeromagnetic dataset. Kahoul et al. (2022) used aeromagnetic data to define the fault system and depth of the basement underlying the Jahamah platform in the northeastern Sirt basin of Libya.

2.2. MAGNETIC DATA PROCESSING

Several grid techniques are developed throughout Oasis Montaj by Geosoft, including Kriging, the minimum curvature technique, random gridding, and bidirectional gridding. These grid techniques can be applied in Oasis Montaj to interpolate data from various geoscientific sources, such as geophysical surveys, geological observations, or geochemical analyses. In contrast, the Kriging technique is used to grid a TMI grid (Fig. 3) from the magnetic dataset that can then be reduced to a pole to generate the RTP grid. Commonly, the RTP conversion assumes that the entire magnetization of the majority of rocks coincides with the Earth's main field or is opposite to it (Keller, 1986; Blakely, 1996). The different anomalies are also associated with variations in the susceptibility of subsurface rocks. Analysing a magnetic dataset includes the use of standard reduction algorithms. Aeromagnetic data is processed (Fig. 2) using reduction to the pole, total horizontal gradient analysis, CET grid analysis, power spectrum analysis, tilt derivative, analytical signal, and Euler deconvolution.

• POWER SPECTRUM ANALYSIS

The power spectrum analysis represents one of the most common methods to figure out the depth of magnetic sources. The magnetic maps' power

spectrum is the product of their 2D Fourier transform and complex conjugate (Ghazala et al., 2018). According to Equation (1), it is a function of wavelength for both the s and c directions.

$$E(r, \vartheta) = \langle H(h, r) \rangle \langle S(a, b, r, \vartheta) \rangle \langle C(t, \Phi, r) \rangle \quad (1)$$

Where E represents the total amount of energy (measured in Hz). r and ϑ denote the number (in cycles/distance units) and azimuth (in degrees) of radial waves, respectively; $\langle \rangle$ expresses the ensemble mean, and h denotes the depth (metres); H is the depth factor; S is the horizontal size (width) factor; C is the vertical size (thickness) factor; a and b are associated with the source's horizontal dimensions; and t and Φ are referring to the vertical depth extent of the source.

It is clear that only three factors (H , S and C) are functions of the radial frequency r , thus in the case of profile form, Equation (1) can be written as:

$$\ln E(q) = \ln H(h^*, q) + \ln S(a^*, q) + \ln C(t^*, \Phi, q) + \text{constant} \quad (2)$$

where (h^*, a^*, t^*) the average depth, half width and thickness of the source ensemble.

According to Saibi et al. (2016), this equation demonstrates that contributions from the depths, widths, and thicknesses of the source ensemble can affect the shape of the energy spectral decay curve.

- **HORIZONTAL GRADIENT (THG)**

Using upright contacts, the THG equation (3) indicates the boundaries of the magnetic anomalies. It is anticipated that the geologic contacts in the study region will be more easily discernible after being filtered using the horizontal gradient. The THG approach (Cordell, 1979) can be used to detect susceptibility variations in magnetic data.

$$\text{HG}(x, y) = \sqrt{\left(\frac{\partial g}{\partial x}\right)^2 + \left(\frac{\partial g}{\partial y}\right)^2} \quad (3)$$

where g denotes a magnetic anomaly, $\text{HG}(x, y)$ denotes horizontal gradient's magnitude, and $\partial g/\partial x$ and $\partial g/\partial y$ are partial derivatives of the function g with respect to the variables x and y , respectively.

- **CET GRID ANALYSIS**

The development of the CET Grid Analysis extension demonstrates the commitment of the Centre for Exploration Targeting (CET) at Curtin University to advancing magnetic data analysis techniques. The CET refers to a specific set of algorithms used for analyzing magnetic data. These algorithms are designed to perform several tasks, including locating, enhancing, and vectorizing discontinuities in the magnetic data. Vectorization involves representing the identified discontinuities as vectors or lines, providing a more intuitive representation of the geological structures present in the magnetic data. Discontinuities, such as faults or geological structures, can have a significant impact on the distribution and

behaviour of magnetic anomalies. The development of algorithms within the CET grid by Holden et al. (2012) uses the application of bilateral symmetry feature detection and texture analysis in the identification of magnetic data discontinuities. Identifying and characterizing these features is crucial for understanding the subsurface geology. The CET grid analysis equation is expressed as follows:

$$E = -\sum_{i=1}^n P_i \text{Log } \rho_i \quad (4)$$

After the histogram of n bins is normalised, the probability ρ is determined.

- **ANALYTICAL SIGNAL**

The analytical signal method (El-Ata et al., 2013) estimated the sources as distinct dipping contacts between vast geological sections. Moreover, it is only moderately sensitive to data noise and interference from adjacent sources. The analytic signal technique assumed that magnetic contacts as causative sources. The analytical signal method Equation (5) (Nabighian, 1972), commonly referred to as the "total gradient," has undergone continual improvements and investigations since its initial use (Saibi et al., 2016).

$$|A(x, y)| = \sqrt{\left(\frac{\partial T}{\partial x}\right)^2 + \left(\frac{\partial T}{\partial y}\right)^2 + \left(\frac{\partial T}{\partial z}\right)^2} \quad (5)$$

In this equation, T represents the anomalous magnetic field, $\partial T / \partial x$ and $\partial T / \partial y$ represent its horizontal derivatives, and $\partial T / \partial z$ denotes its vertical derivative.

- **TILT DERIVATIVE**

Qualitative Miller and Singh (1994) and Verduzco et al. (2004) proposed the analytic signal approach, which was refined by the tilt derivative method, also called the tilt angle method. The tilt-angle method was utilised to sharpen and enhance the magnetic anomalies. Using a set of horizontal and vertical derivatives of the magnetic field, a tilt angle derivative is performed to distinguish between these two types of anomalies (Ming et al., 2021). When the TDR value is positive, it shows a positive contrast with the underlying causative source, whereas when it is negative, it indicates that it is outside the limits of the source.

$$\text{TDR} = \tan^{-1} \left\{ \frac{\frac{\partial T}{\partial z}}{\sqrt{\left(\frac{\partial T}{\partial x}\right)^2 + \left(\frac{\partial T}{\partial y}\right)^2}} \right\} \quad (6)$$

Where T represents the observed magnetic field at (x, y) and the horizontal and vertical derivatives of F ($\partial T/\partial x$), ($\partial T/\partial y$), and ($\partial T/\partial z$), respectively.

- **EULER DECONVOLUTION**

Euler deconvolution estimates source depth and location for various homogeneous magnetic sources. A structural index (Table 1) is an exponential variable

Table 1 Structural index for magnetic (FitzGerald et al., 2004).

| Source | Magnetic |
|------------|----------|
| Sphere | 3 |
| Horizontal | 2 |
| Fault | 1 |
| Contact | 0 |

that explains the nature of geologic bodies. This technique is particularly helpful in interpreting magnetic data because it involves such little basic knowledge about the source body's structure (Thompson, 1982; Reid et al., 1990).

The Euler deconvolution in 3D Equation (7) is expressed as follows:

$$N(B - T) = (x - x_0) \left(\frac{\partial T}{\partial x} \right) + (y - y_0) \left(\frac{\partial T}{\partial y} \right) + (z - z_0) \left(\frac{\partial T}{\partial z} \right) \quad (7)$$

where T represents the field measured at locations (x, y, and z). $x_0, y_0,$ and z_0 represent coordinates of the source site; B represents the baseline level of the field (regional value at x, y, and z); and N represents the structural index or homogeneity degree that is a function of the source geometry of the causative bodies.

3. RESULTS AND DISCUSSION

The total magnetic intensity map (Fig. 3) shows high anomalies in the northwest, southeast, and east parts of the region, which may be the imprint of the high magnetic susceptibility and be associated with Cenozoic volcanic rocks in the region. Further, these high values of NW-SE are characterised by the Garyan-Tarhona uplift in the upper Cretaceous or

lower Tertiary, resulting in anticlinal swelling. The northeast and southwest parts of the region are indicated by low magnetic anomalies, which are characterised by low magnetic susceptibility. These low magnetic values refer to surrounding areas when grabens formed in the NE-SW along marginal parts of the uplifts during the Jurassic/Triassic-Jurassic (Saadi et al., 2008). The magnetic data has magnitudes ranging from 34 to 110 nT. Magnetic data is reduced to the pole to isolate magnetic anomaly field areas. The values -30.06 degrees and -4.73 degrees, respectively, were used for inclination and declination in order to correct the inappropriate distortion in the sizes, shapes, and positions of magnetic anomalies resulting from the inclination of the magnetic field of the earth.

The reduction to the pole map (Fig. 4) shows magnetic values ranging from 17 nT to 172 nT. Within the RTP map, the magnetic source directly lies below anomalies. The west and southeast parts of the area show high magnetic anomaly values, ranging from 50 nT to 172 nT, whereas low magnetic anomaly values are indicated in the central and northeast parts, ranging from 17 nT to 35 nT. These strong, high anomaly values are associated with Tertiary-Quaternary volcanic rocks that cover most of the study region. The lower values in the central part of the area refer to basins with thick sediment deposited, which are related to tectonic events in the late Jurassic and upper Cretaceous.

The power spectrum analysis is applied to the magnetic data to identify the dominant frequencies or spatial scales associated with the magnetic sources. Two distinct magnetic sources have been identified, and their depths have been estimated using power spectrum analysis (Fig. 5). The shallow source has a depth estimated at around 3 km, whereas the deep

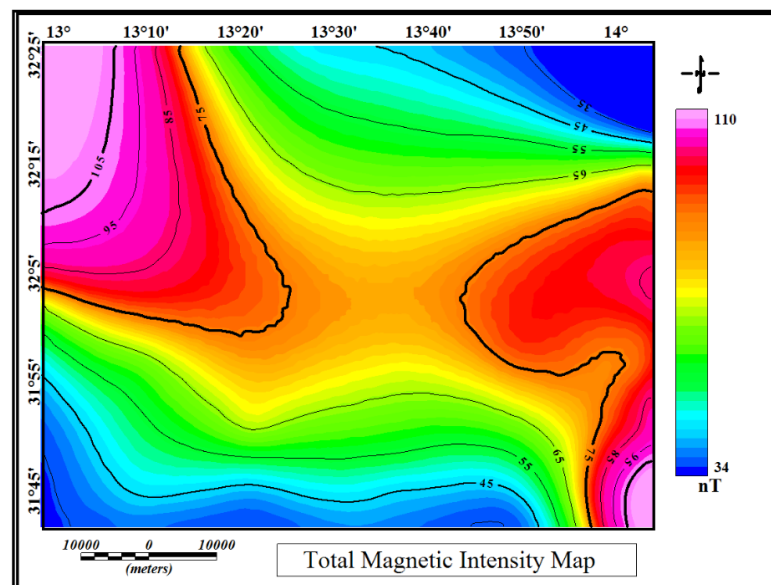


Fig. 3 Total magnetic intensity map of Tarhona area.

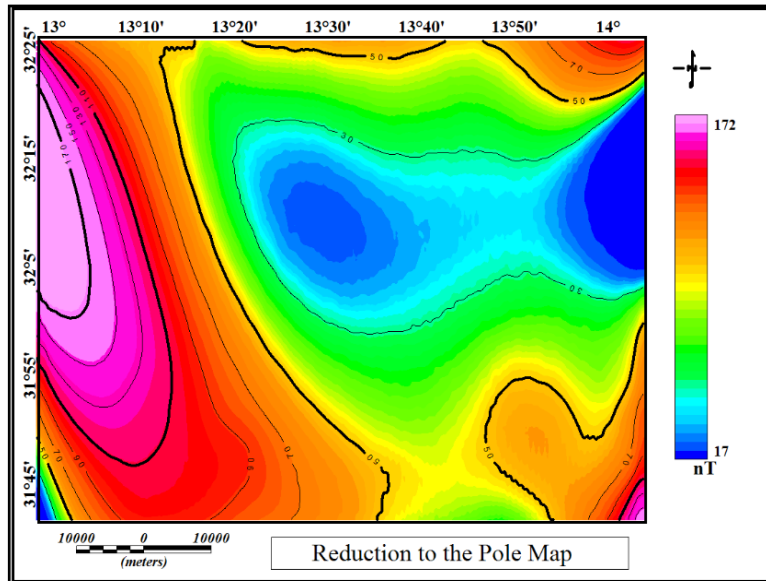


Fig. 4 Reduction to the pole map.

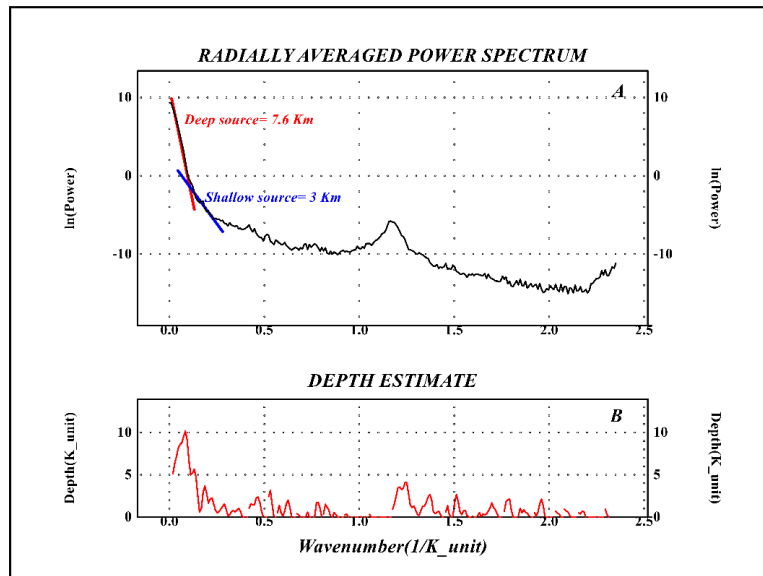


Fig. 5 (a) The radially average energy spectrum of the Tarhona region's magnetic data; (b) Depth estimation of the magnetic source.

source is indicated at approximately 7.6 km from the next equation: $H = -S/4$. Where H is the depth and S is the slope of the log (energy) spectrum.

Within the CET grid analysis, the smallest filter wavelength was set to 4 cells, the number of filters was scaled to 4, and the value of congruency strength was set at 5. The results of the CET grid analysis and total horizontal gradient map (Figs. 6a, b) show a positive amplitude that delineates the subsurface elements of the study region, with major trends N-S, NNW-SSE, and NW-SE. These trends are the result of different tectonic events. The N-S fault trend associated with structural development in the NW African basin was periodically reactivated as strike-slip faults that occurred in the early Caledonian and Hercynian tectonic events, according to Klitzsch (1970), and may be due to the similar tectonic event that caused the

Nafusah Arc. The NNW-SSE fault trend is related to the reactivation of Cretaceous lineaments in the Hun Graben. The NW-SE fault is associated with the movement of the African and European collisions in the Hercynian event (upper Cretaceous or lower Tertiary).

The amplitude of the AS (analytic signal) peaks (Fig. 7) is used to determine the locations where the magnetic anomalies are most pronounced. The peaks correspond to areas where the magnetic field strength deviates significantly from the background or regional magnetic field. By selecting the AS maxima (peaks), which represent the highest values of the amplitude, the boundaries or edges of the magnetic sources can be delineated. The values that are high in the southeast, northeast, northwest, and west of the region are reflected as a high AS for magnetic data, which

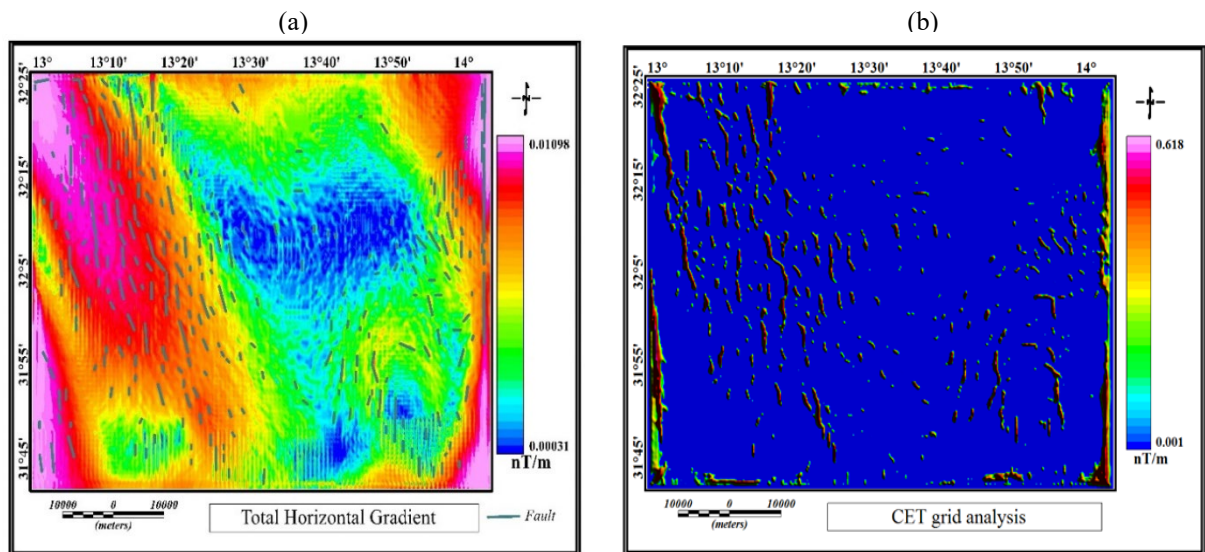


Fig. 6 (a)Total Horizontal gradient map;(b) CET grid analysis of RTP.

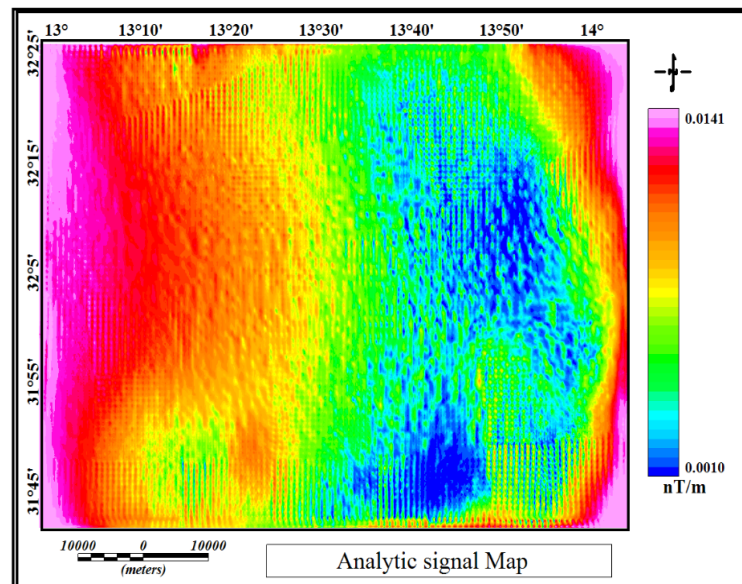


Fig. 7 Analytic signal map of RTP Map.

indicates that all of these areas include important magnetic susceptibility variations that form distinguishable elements within this map.

The magnetic anomaly in Oasis Montaj is utilised to create Euler deconvolution maps. A value of 1.0 was set for the structural index in order to figure out the best solutions that could be achieved. Furthermore, structural index = 1.0 yields superior solutions compared to SI = 2 and SI = 3 since these data are clustered in a few key locations rather than being randomly distributed across the study region. In addition, the solution of structural index = 1.0 provides the main faults superimposed on the magnetic anomaly's edge. The window size of 7x7 and the solution with a structural index of 1.0 for a maximum depth tolerance of 18 % were applied within the Euler deconvolution. Euler deconvolution techniques with

the TDR method identify the most probable locations and depths of the subsurface sources. In the results of the Euler deconvolution applied to the magnetic anomaly data (Fig. 8), it is observed that the depths of the faults within the studied area exhibit a range from 2000 metres to over 8000 metres. Furthermore, these faults display distinct trends, namely N-S (north-south), NNW-SSE (north-northwest to south-southeast), and NW-SE (northwest to southeast). The dominant N-S trend is commonly found along the eastern part of the study area, while the NNW-SSE and NW-SE trends are mostly located in the western area of the region. The rose diagram identified the main fault trending in the N-S, NNW-SSE, and NW-SE directions (Fig. 9). The Euler solution map confirmed the trend faults observed in the THG, AS, CET, and TDR. Numerous circular forms that might be

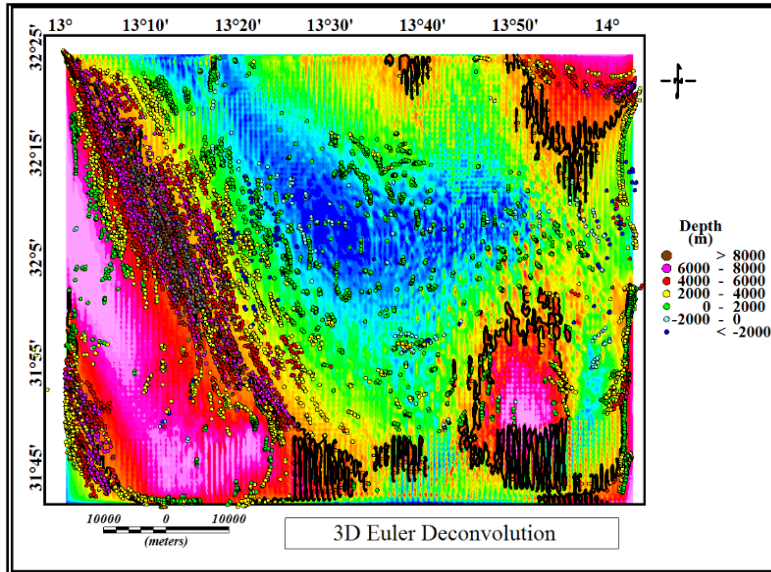


Fig. 8 3D Euler deconvolution map ($W=7$, $SI=1$) with the tilt angle derivative.

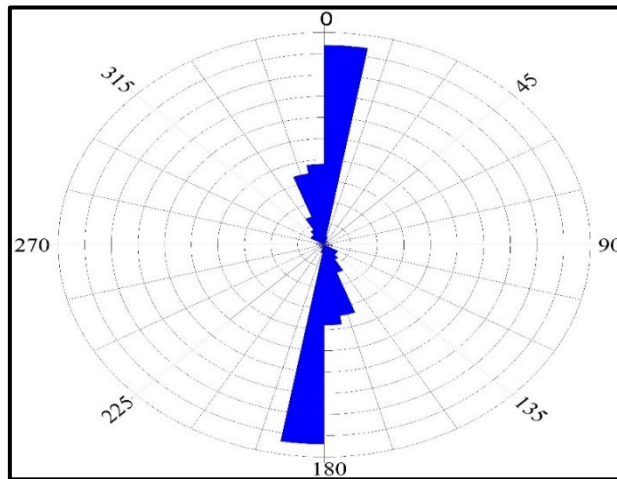


Fig. 9 Rose diagram of the main faults extracted from THG, CET, AS, TDR, and 3D-Euler deconvolution methods.

associated with underground intrusion bodies are observed among the Euler solutions, which are grouped along the predominant faults.

The TDR (tilt angle derivative) is created after applying a filter to the RTP map. The zero-contour line that appears at or near contact can be seen more clearly with a tilt derivative. If the TDR value is positive, it means that there is a good contrast with the underlying causative source, whereas if it is negative, it denotes that the effect is not limited by the source. Tilt-angle filters typically locate anomalies at or near their sources of origin. The magnitudes of these anomalies (Fig. 10) range from -1.4 to 1.2 degrees, as observed on the map. The negative and positive values represent the direction and extent of the anomalies. The TDR of the RTP shows fault trends N-S, NW-SE, and NNW-SSE. The findings are consistent with the results of previous studies conducted by Goudarzi (1981) and Saadi et al. (2008).

4. CONCLUSION

The fault system trends with their source depths are delineated in the Tarhona region of NW Libya using a variety of analytical methods applied to the magnetic dataset, including total horizontal gradient, CET grid analysis, power spectrum, analytical signal, Euler deconvolution, and tilt derivative. The high anomaly value was identified from reduction to the pole map with a range of 172 nT. Fault trends (N-S, NW-SE, and NNW-SSE) obtained from the total horizontal gradient, CET grid, analytic signal, and tilt angle derivative of the RTP map show similar dominant trends as those indicated from Euler deconvolution. These trends were attributed to tectonic activity during the upper Cretaceous and Cenozoic tectonic movements during the Caledonian and Hercynian events that were associated with North African structural development. Euler deconvolution techniques with TDR estimated the depth of the source bodies between 2000 and 8000 m. The magnetic data

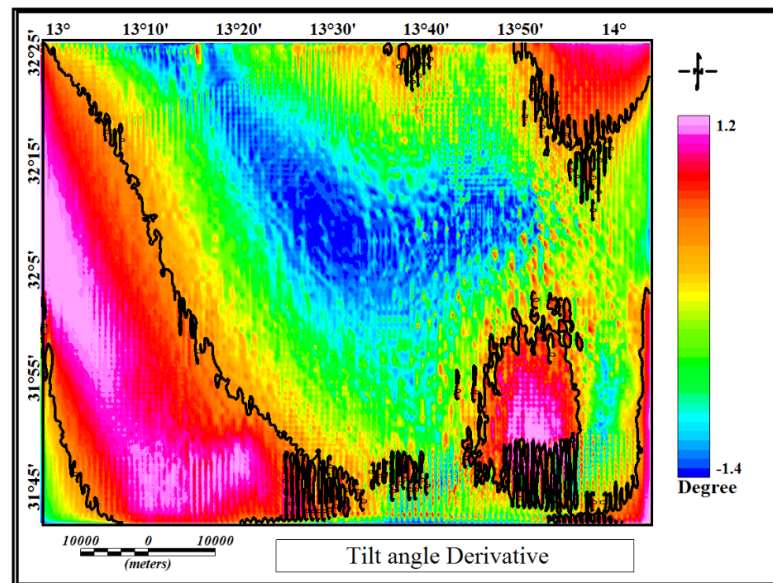


Fig. 10 Tilt angle derivative map.

interpretation can provide a real image of the subsurface structure that was previously unknown and reduce the ambiguity of geological interpretation within the area. Furthermore, pinpointing these faults is crucial for clarifying geological interpretations and expanding our understanding of the study area's prevailing trends, which can be utilised in future exploration.

ACKNOWLEDGEMENTS

"Acknowledgement to the Higher Education Malaysia Ministry through the Fundamental Research Grant Scheme [Project Code]." Project Code: FRGS/1/2022/STG08/USM/03/1 entitles "Performance-Based Multimodal Geophysical Design for Soil Dynamic Properties to Improve Visualisation of Subsurface Conditions." Additionally, a research university grant entitles "Integrated geophysical characterization of geothermal exploration and strategy for the sustainable use of geothermal resources" with account no. 1001/PFIZIK/8011110.

REFERENCES

Abdulkadir, Y.A., Fisseha, S. and Jothimani, M.: 2022, Digital elevation model and satellite gravity anomalies and its correlation with geologic structures at Borena basin, in the Southern Main Ethiopian Rift. DOI: 10.1080/22797254.2022.2130096

Abohajar, A., Krooss, B., Harouda, M. and Littke, R.: 2009, Maturity and source-rock potential of Mesozoic and Palaeozoic sediments, Jifarah Basin, NW Libya. *J. Pet. Geol.*, 32, 4, 327–341. DOI: 10.1111/j.1747-5457.2009.00453.x

Alfandi, E.: 2012, Early Mesozoic stratigraphy, sedimentology and structure of the Gharian area, north-western Libya. Ph. D Thesis, University of Plymouth. DOI: 10.24382/3376

Anketell, J.: 1996, Structural history of the Sirt basin and its relationship to the Sabrata basin and Cyrenaica platform, northern Libya. *The Geology of the Sirt Basin, III*, Elsevier, 57–89.

Antonovic, A.: 1977, Geological map of Libya 1/250 000, Mizdah. Industrial Research Centre, Tripoli, Socialist People's Libyan Arab Jamahiriyyah, sheet NH, 33–31.

Anudu, G.K., Stephenson, R.A. and Macdonald, D.I.: 2014, Using high-resolution aeromagnetic data to recognise and map intra-sedimentary volcanic rocks and geological structures across the Cretaceous middle Benue Trough, Nigeria. *J. African Earth Sci.*, 99, 2, 625–636. DOI: 10.1016/j.jafrearsci.2014.02.017

Blakely, R.J.: 1996, Potential theory in gravity and magnetic applications, 34. Cambridge University Press, New York, 441 pp. DOI:10.1017/CBO9780511549816

Capitanio, F., Faccenna, C., Funicello, R. and Salvini, F.: 2011, Recent tectonics of Tripolitania, Libya: an intraplate record of Mediterranean subduction. *Geol. Soc. Spec. Publ.*, 357, 1, 319–328. DOI: 10.1144/SP357.17

Christie, A.M.: 1966, Geology of the Garian Area, Tripolitania, Libya. Geological section, Ministry of Industry. Bull. 5, 60 pp.

Cordell, L.: 1979, Gravimetric expression of graben faulting in Santa Fe Country and the Espanola Basin, New Mexico. Paper presented at the New Mexico Geological Society. Guidebook: 30th Field Conference, New Mexico, 59–64.

El-Ata, A.S.A., El-Khafeef, A.A., Ghoneimi, A.E., Abd Alnabi, S.H. and Al-Badani, M.A.: 2013, Applications of aeromagnetic data to detect the Basement Tectonics of Eastern Yemen region. *Egypt. J. Pe.*, 22, 2, 277–292. DOI: 10.1016/j.ejpe.2013.06.007

El Hinnawy, M. and Cheshitev, G.: 1975, Geological Map of Libya. Tarabulus (NI33-13). Explanatory Booklet. Ind. Res. Cent., Tripoli.

Eldosouky, A.M.: 2019, Aeromagnetic data for mapping geologic contacts at Samr El-Qaa area, north Eastern Desert, Egypt. *Arab. J. Geosci.*, 12, 1, 1–13. DOI: 10.1007/s12517-018-4182-2

- Elkhateeb, S.O., Eldosouky, A.M. and Samir, A.: 2018, Interpretation of aeromagnetic data to delineate structural complexity zones and porphyry intrusions at Samr El Qaa Area, North Eastern Desert, Egypt. *Int. J. Novel Res. Civ. Struct. Earth Sci.*, 5, 1, 1–9.
- Farahat, E., Ghani, M.A., Aboazom, A. and Asran, A.: 2006, Mineral chemistry of Al Haruj low-volcanicity rift basalts, Libya: implications for petrogenetic and geotectonic evolution. *J. African Earth Sci.*, 45, 2, 198–212. DOI: 10.1016/j.jafrearsci.2006.02.007
- Fatmi, A.N., Sbata, A.M. and Eliagoubi, B.A.: 1978, Guide to the Mesozoic stratigraphy of Jabal Nefusa, Libyan Jamahiriya, Arab Development Institute. Publication No. 7, 35pp.
- Feumoe, A.N.S., Ndougsa-Mbarga, T., Manguelle-Dicoum, E. and Fairhead, J.D.: 2012, Delineation of tectonic lineaments using aeromagnetic data for the south-east Cameroon area. *Geofizika*, 29, 2, 175–192.
- FitzGerald, D., Reid, A. and McInerney, P.: 2004, New discrimination techniques for Euler deconvolution. Paper presented at the 8th SAGA Biennial Technical Meeting and Exhibition. DOI: 10.1016/j.cageo.2004.03.006
- Ghazala, H.H., Ibraheem, I.M., Lamees, M. and Haggag, M.: 2018, Structural study using 2D modeling of the potential field data and GIS technique in Sohag Governorate and its surroundings, Upper Egypt. *NRIAG J. Astron. Geophys.*, 7, 2, 334–346. DOI: 10.1016/j.nrjag.2018.05.008
- Giraudi, C.: 2005, Eolian sand in peridesert northwestern Libya and implications for Late Pleistocene and Holocene Sahara expansions. *Palaeogeogr. Palaeoclimatol. Palaeoecol.*, 218, 1-2, 161–173. DOI: 10.1016/j.palaeo.2004.12.014
- Goudarzi, G.H.: 1981, Structure – Libya. In: Salem, N.J. and Busrewil, M.T. (eds), 2nd Symposium on Geology of Libya, 3, Academic Press, London, 879–892.
- Hallett, D. and Clark-Lowes, D.: 2017, Petroleum geology of Libya, Elsevier.
- Hinze, W., Von Frese, R.R. and Saad, A.H.: 2013, Gravity and Magnetic Exploration: Principles, Practices, and Applications. Cambridge University Press.
- Kahoul, S., Sidek, A., Eshanibli, A., Trepil, F., Jaafar, M.Z.B., Hassan, M. and Dugdug, L.: 2022, Identifying fault system and basement depth using aeromagnetic data Beneath the Jahamah Platform, NE Sirt Basin, Libya. *Acta Geodyn. Geomat.*, 19, 2, 155–166. DOI: 10.13168/AGG.2022.0005
- Keller, G.V.: 1986, An introduction to geophysical exploration. *EOS Trans. AGU*, 67, 11, 132–132. DOI: 10.1029/EO067i011p00132-01
- Klitzsch, E.: 1970, The structural history of the Central Sahara: New insights into the structure and palaeogeography of a plateau. *Geological Review*, 59, 459–527, (in German).
- Klitzsch, E. and Gray, C.: 1971, The structural development of parts of North Africa since Cambrian time. Paper presented at the Symposium on the geology of Libya: Tripoli, Faculty of Sciences, University of Libya, 256–260.
- Mann, K.: 1975, Explanatory Booklet, Sheet: Al Khums, NI 33-14. Geological map of Libya. Libyan Arab Republic, Industrial Research Centre Tripoli, 1-80.
- Masoud, A.A. and Koike, K.: 2011, Auto-detection and integration of tectonically significant lineaments from SRTM DEM and remotely-sensed geophysical data. *ISPRS J. Photogramm. Remote Sens.*, 66, 6, 818–832. DOI: 10.1016/j.isprsjprs.2011.08.003
- Miller, H.G. and Singh, V.: 1994, Potential field tilt - a new concept for location of potential field sources. *J. Appl. Geophys.*, 32, 2-3, 213–217. DOI: 10.1016/0926-9851(94)90022-1
- Ming, Y., Ma, G., Li, L., Han, J. and Wang, T.: 2021, The spatial different order derivative method of gravity and magnetic anomalies for source distribution inversion. *Remote Sens.*, 13, 5, 964. DOI: 10.3390/rs13050964
- Nabighian, M.N.: 1972, The analytic signal of two-dimensional magnetic bodies with polygonal cross-section: Its properties and use for automated anomaly interpretation. *Geophysics*, 37, 3, 507–517. DOI: 10.1190/1.1440276
- Piccoli, G.: 1970, Outlines of volcanism in northern Tripolitania (Libya). *Boll. della Soc. Geol. Ital.*, 89, 449–461.
- Reid, A. and Allsop, J.G.H., Millet, A. and Somerton, I.: 1990, Magnetic interpretation in three dimensions using Euler Deconvolution. *Geophysics*, 55, 80–91. DOI: 10.1190/1.1442774
- Rusk, D.C.: 2001, Libya: Petroleum potential of the underexplored basin centers – A twenty-first-century challenge. *AAPG Memoir* 74, 429–452.
- Saadi, N.M., Aboud, E., Saibi, H. and Watanabe, K.: 2008, Integrating data from remote sensing, geology and gravity for geological investigation in the Tarhunah area, Northwest Libya. *Int. J. Digit. Earth*, 1, 4, 347–366.
- Saadi, N.M., Zaher, M.A., El-Baz, F. and Watanabe, K.: 2011, Integrated remote sensing data utilization for investigating structural and tectonic history of the Ghadames Basin, Libya. *Int. J. Appl. Earth Obs. Geoinf.*, 13, 5, 778–791. DOI: 10.1016/j.jag.2011.05.016
- Saibi, H., Azizi, M. and Mogren, S.: 2016, Structural investigations of Afghanistan deduced from remote sensing and potential field data. *Acta Geophys.*, 64, 4, 978–1003. DOI: 10.1515/acgeo-2016-0046
- Salehi, R., Saadi, N.M., Khalil, A. and Watanabe, K.: 2015, Integrating remote sensing and magnetic data for structural geology investigation in pegmatite areas in eastern Afghanistan. *J. Appl. Remote Sens.*, 9, 1, 096097. DOI: 10.1117/1.JRS.9.096097
- Sharma, P.V.: 1997, Environmental and engineering geophysics. Cambridge University Press, 475 pp. DOI: 10.1017/CBO9781139171168
- Thompson, D.: 1982, EULDPH: A new technique for making depth estimates from magnetic data computer assisted depth estimates from magnetic data. *Geophysics*, 47, 31–37. DOI: 10.1190/1.1441278
- Trepil, F., Kahoul, S., Uyimwen, O.A., Eshanibli, A., Ismail, N.A., and Ghanoush, H.: 2021, Delineation of structure elements and the basement depth at the Jifara Plain NW Libya using integration application of potential field dataset. *Acta Geodyn. Geomat.*, 18, 1, 83–90. DOI: 10.13168/AGG.2021.0006
- Vasanthi, A., Sharma, K. and Mallick, K.: 2006, On “New standards for reducing gravity data: The North American gravity database” (W.J. Hinze et al., 2005, *Geophysics*, 71, J25–J32). *Geophysics*, 71, 6, X31–X32. DOI: 10.1190/1.2361084
- Verduzco, B., Fairhead, J.D., Green, C.M. and MacKenzie, C.: 2004, New insights into magnetic derivatives for structural mapping. *Lead. Edge*, 23, 2, 116–119. DOI: 10.1190/1.1651454
- Zivanovic, M.: 1977, Geological Map of Libya. Explanatory Booklet, Sheet Bani Walid NH 33-2. Industrial Research Center, Tripoli, Libya.